A new integrated optical angular velocity sensor

Caterina Ciminelli [(1)], Benedetto Bandini [(1)], Francesco Peluso [(1)], Nicola Catalano [(2)], Errico Armadillo [(3)], Mario N. Armenise [(1)]

(1) Dipartimento di Elettrotecnica ed Elettronica, Politecnico di Bari,
Via Re David, 200 – 70125 Bari, Italy
c.ciminelli@poliba.it

(2) RAF srl,
Via Peucetia, 21/D – 70125 Bari, Italy
catalano.n@libero.it

(3) ESA-ESTEC,
Keplerlaan 1 - Postbus 299, 2200 AG Noordwijk, The Netherlands
errico.armandillo@esa.int

INTRODUCTION

Guidance, navigation or control systems in aircrafts and spacecrafts, and attitude systems in terrestrial vehicles require more compact, low cost and more reliable gyroscopes. For this reason, angular velocity sensors are key elements, which are essential to obtain the desired sensitivity for the control and stabilization of the carrier attitude.

Gyros having a sensitivity in the range 10 – 100 °/s are required in both space and terrestrial vehicles navigation systems. Attitude and heading systems in aircrafts and precision inertial navigation systems require a different gyro sensitivity 1 °/s, and 0.01 – 0.001 °/s, respectively.

Currently, the most widely used gyro technology for high performance gyro systems is the optical fiber-based technology. However, although some research efforts have been spent on new technologies able to produce very compact, low-cost and high-performance angular velocity sensors, much work has to be done to prove the potential of new devices. In particular, integrated optical angular velocity sensors (AVSs) are very promising in terms of performance parameters such as low cost, compactness, light weight and high reliability.

Integrated optical AVSs are based on the Sagnac effect, which generates a phase or frequency difference proportional to the angular velocity when two light beams counter-propagating in an optical resonant cavity suffer a rotation.

Sagnac effect has been demonstrated in semiconductor ring laser-based AVSs [1-2]. Passive integrated optical AVS with the laser source external to the ring resonator, are particularly attractive because they show high performance and overcome some issues of the active devices, i.e. lock-in effect and mode competition.

In this paper, the one-axis integrated optical gyroscope using the integrated optical angular velocity sensor based on a passive resonant configuration is proposed. The AVS is formed by a waveguiding ring resonator in which a couple of semiconductor optical amplifiers are integrated, and two external symmetrical arms, each of them including a laser source, a frequency shifter, a polarization controller, an optical isolator and a photodiode [3]. The sensor has to operate under traveling-wave conditions.

In the following sections a brief description of the passive ring resonator gyro technology and main characteristics of the new integrated optical devices are reported.

PASSIVE RING RESONATOR-BASED GYROSCOPES (PRRGs)

In this section we briefly report on the passive ring resonator gyros proposed in literature.

A cavity formed by two highly reflective mirrors and two partially transmitting mirrors (one at the input and the other at the output) is a simple configuration of a passive ring resonator angular velocity sensor to be used in PRRGs. An integrated configuration of PRRG is formed by an optical cavity coupled to the input and output by means of two optical couplers. The two counter-propagating beams in the resonant ring are generated by two external lasers or by one laser and a beam splitter and are frequency matched with the resonant frequencies usually using two acousto-optic frequency shifters.

PRRGs are frequency sensitive devices in which the frequency difference between two resonant counter-propagating beams is generated by the Sagnac effect under rotation conditions.

The measurement uncertainty depends on the resonator geometry, resonator linewidth and on the device signal-to-noise ratio (SNR).

High sensitivity (no gain variations in the laser are expected), low cost, mechanical stability (no moving parts), low power consumption, high polarization selection and high reliability are the advantages shown by PRRGs. The main disadvantage of this technology is the need of using low-loss waveguide materials and large ring radius to obtain high finesse and low quantum limit. For these reasons most of the proposed devices are not useful for high performance space applications.

In [4] an optical resonant gyro where the sensing element is an integrated optic waveguide is reported. Rate response in the range 1-200 °/s has been achieved with a theoretical angle random walk of 0.1 °/√h. The study of the cavity element for a resonant micro optic gyroscope has been proposed in [5]. The resonator consists of a circular waveguide fabricated by ion-beam deposition, designed to get a finesse equal to 300 without any compensation. An integrated resonator-based gyroscope, monolithically integrated on a silica planar lightwave circuit is reported in [6]. This device has been modelled taking into account also some countermeasures for backscattering induced noise and polarization fluctuation induced noise. The sensitivity, calculated considering only the shot noise at the detector, was 2.9 10^{-3} °/s. A gyroscope based on a double-arm, integrated optic ring resonator fabricated by ion exchange in glass is discussed also in [7,8]. The shot noise limited performance is 0.3 °/√h.

In [3,9,10] we already proposed preliminary results on the integrated optical angular velocity sensor having the resonant configuration discussed in this paper. The device performance have been evaluated in case of non compensated, fully compensated and partially compensated losses of the resonator and for different operating wavelengths. A perfectly circular configuration of the resonator has been assumed. The analysis has been carried out by changing the ring radius, the input power and the coupling coefficient having 0.5 °/h as a target specification. Preliminary results encouraged us to perform deeper analysis and to continue with the fabrication of a first prototype which is now in progress. In this paper, we propose new results obtained from the of the sensor configuration before proceeding to the breadboard fabrication. First of all, our choice has been oriented towards a low loss material, like a silica-based one, with the aim of realizing a device with a sufficiently high quality factor without any loss compensation. Furthermore, the need of a high coherence laser source, like DFB lasers used in WDM telecommunication systems, together with the low-loss waveguide requirement, has focused the analysis on the operating wavelength equal to 1.55 μm. The AVS under analysis is targeted at high performance space applications with sensitivity requirement of a few °/h. The calculations we made for the perfectly circular resonator without any loss compensation have demonstrated a sensitivity value worse than the current target one. This is the reason why we are considering a sensor configuration with integrated optical amplifier for compensation purposes. Since the sensitivity value strongly depends on the ratio perimeter/area, L/A, of the resonator and we do not need to reach a trade-off between losses and L/A value in case of fully compensated loss device, we studied a resonator geometry, different from the circular one, which can allow getting a lower value of L/A.

NEW CONFIGURATION

In this section the new passive configuration of an integrated optical angular velocity sensor to be used in PRRGs is described.

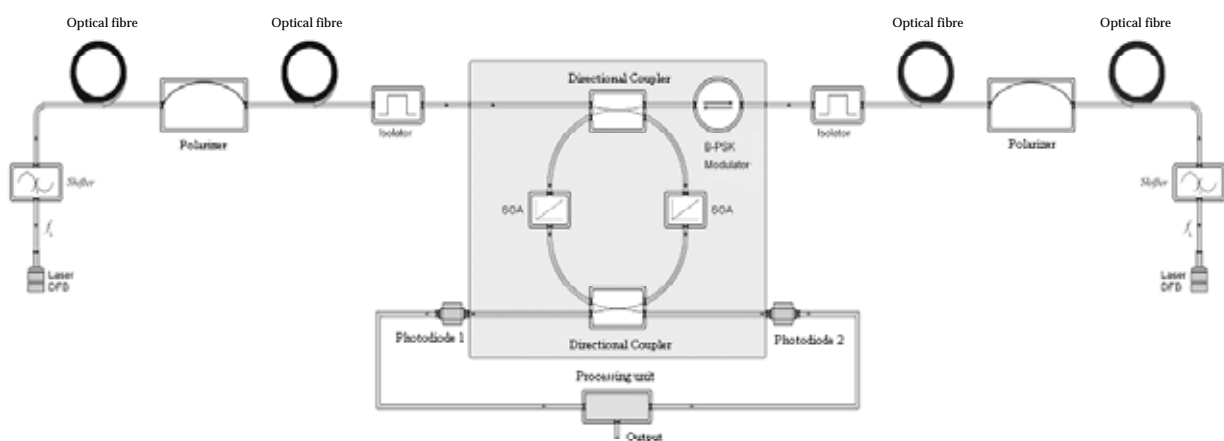Fig.1 reports the conceptual scheme of the sensor.

Fig. 1. Scheme of the integrated optical AVS

The sensor chip includes a waveguiding ring resonator, in which two integrated SOAs are symmetrically placed, two directional couplers, two straight passive waveguides and a BPSK modulator. The device includes also two symmetrical external branches each of them formed by a DFB laser, a frequency shifter, a polarization controller and an optical isolator. Polarization maintaining fibers and external photodiodes are also required. The two beams coming from the laser sources are separately coupled to the ring resonator through the upper coupler, counter-propagate in the ring if the frequency of each beams is equal to one of the resonance frequencies and are extracted at the lower coupler. Polarization maintaining fiber and polarization controller are included to reduce the effects of the polarization fluctuation. Any increase of the path length generates a change in the resonant frequencies and a decrease of the free spectral range. To mach the laser source frequency and the resonant frequency, external shifters or tunable lasers have to be used.

At the resonance conditions, if the total losses in the ring are fully compensated by the SOAs, the travelling-wave operation is realized, which means that under the steady-state regime, the transfer function of the ring is equal to 1. The losses due to the propagation in the external waveguides and to the components in each external branch can be compensated by appropriately choosing the value of the laser output power. The loss at the directional couplers affects only the transient regime, which has been evaluated [3] of the order of μs, while, under steady-state conditions, it only modifies the resonant linewidth.

Best performance for such devices can be achieved when reciprocity in the structure is guaranteed. This implies that SOAs are placed symmetrically with respect to the couplers and both couplers have the same coupling efficiency.

The use of SOAs allows the reduction of the resonant mode linewidth Γ and, therefore, of the minimum measurable angular velocity $\delta\Omega$, which is expressed as:

$$\delta\Omega = \frac{\lambda_0 L}{4A} \frac{\sqrt{2}}{SNR} \Gamma \tag{1}$$

where λ_0 is the resonant mode wavelength, L the ring perimeter, and A the ring area. Γ can be expressed by $\Gamma = f_0/Q$, with f_0 resonant frequency, and Q is the quality factor of the resonator.

To reduce the measurement uncertainty $\delta\Omega$, Γ needs to be decreased, that is it needs to increase Q (or reduce losses) at a fixed resonant frequency. When the losses in the ring are fully compensated, the quality factor and, then, $\delta\Omega$ will be affected only by the coupling coefficient η of the couplers. The SNR can be evaluated by calculating the photocurrent and the noise contribution at the detector; it also depends on η. We have already demonstrated [3,9,10] that the value of the coupling efficiency must be very low (~ 0.2 %) to achieve very high performance ($\delta\Omega < 1$ °/h).

In [3,9,10] we reported on the results obtained for a perfectly circular geometry of the resonator. As already mentioned, since for fully compensated devices the sensitivity is improved by reducing the ratio L/A, we have also considered different geometries of the resonator. Fig. 2 shows the ring geometry for which we obtained the best performance of the sensor.
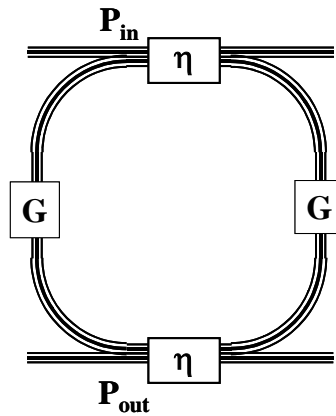

Fig. 2. "Square" geometry of the resonator

The device transfer function has been obtained by assuming as perfectly coherent (i.e. random phase fluctuation equal to zero) beams coming from the laser sources. Temporal coherence of the light source can be also taken into account in the analysis, even if no significant variations have been already demonstrated [3,9,10] when a coherence value as high as possible (> 0.85) is assumed. This value of the coherence parameter is achievable for state-of-art DFB lasers.

Fig. 3 reports the transfer function for three different values of the coupling coefficient and the same value of the area enclosed in the optical path. It can be clearly observed that the change is not relevant for losses fully compensated. On the contrary, without any losses compensation, the linewidth of the resonant mode is increased, as it is shown in Fig. 4, and this, in turn, causes a decrease of the sensitivity.
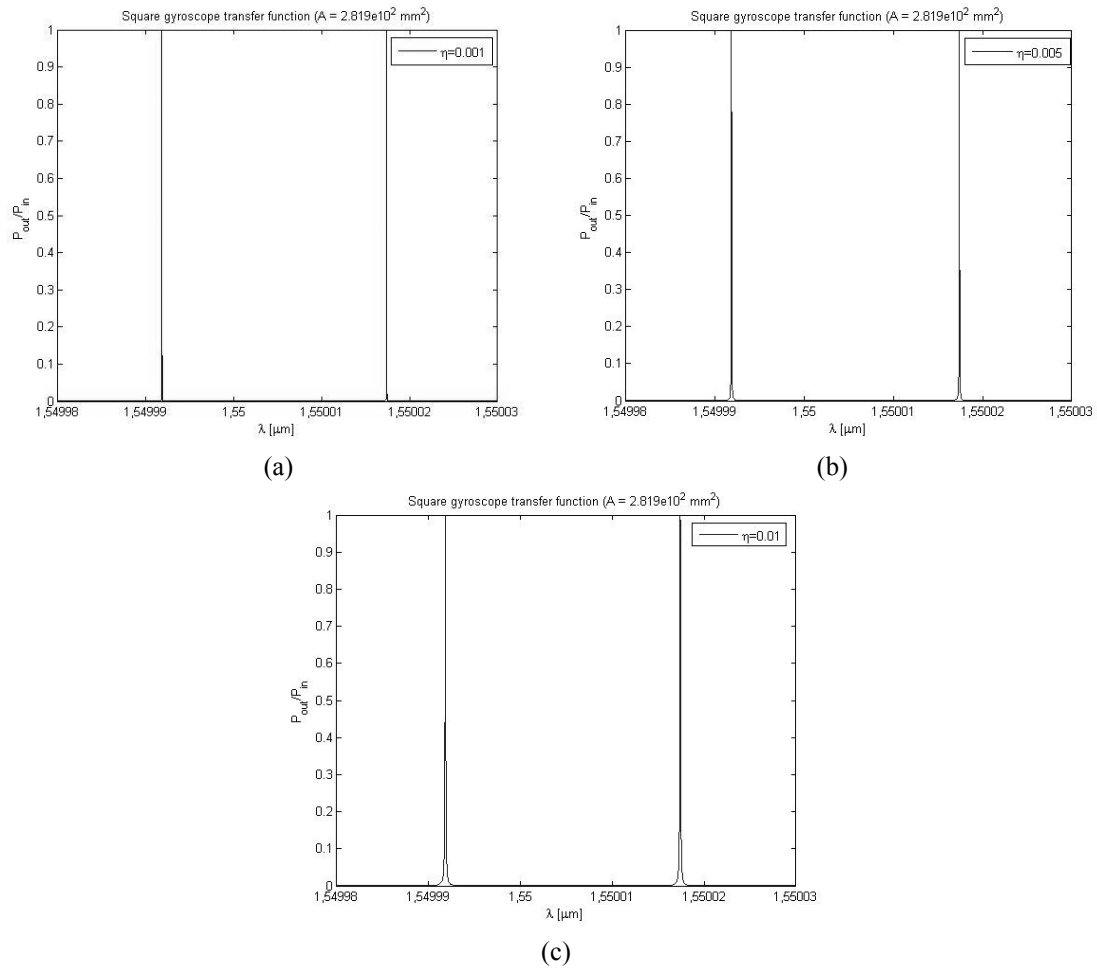

(a)

(b)

(c)

Fig. 3. Transfer function with (a) η = 0.001, (b) η = 0.005, (c) η = 0.01; A = 2.819 10^2 mm^2 at λ = 1.55 μm; full losses compensation
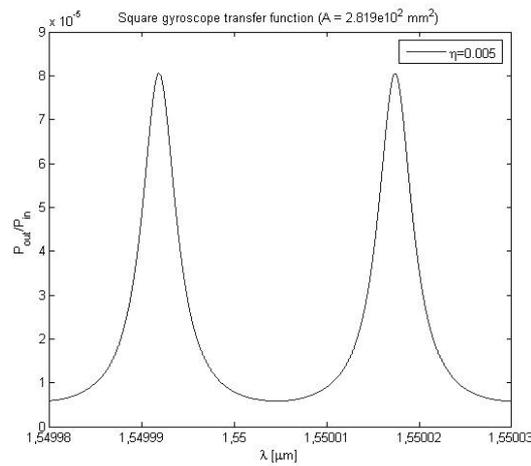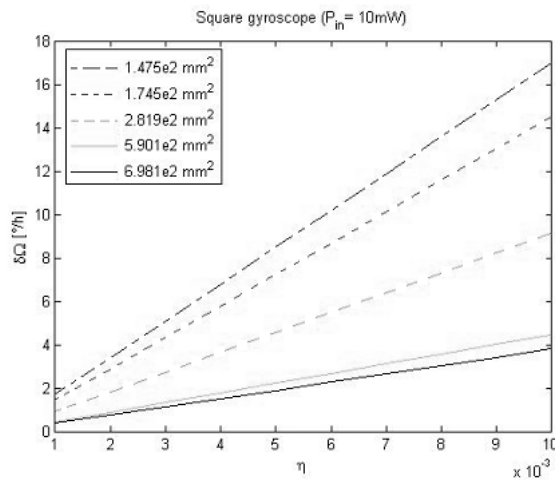

Fig. 4. Transfer function with η = 0.005, A = 2.819 10^2 mm^2 at λ = 1.55 μm; no losses compensation
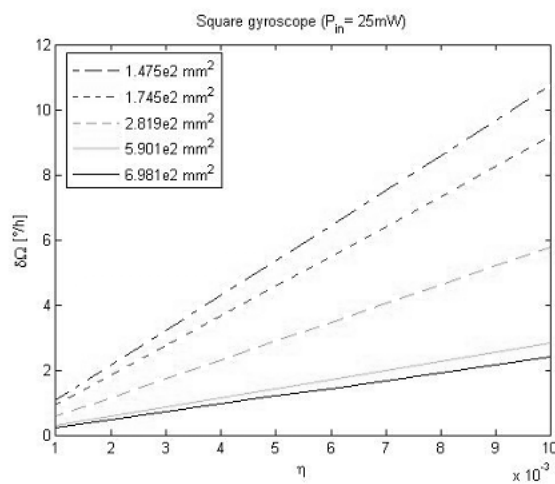
In Fig.5a, b, and c sensitivity is reported as a function of the coupling coefficient at λ = 1.55 μm for different values of ring area A and input power P_{in} = 1 mW, P_{in} = 10 mW and P_{in} = 25 mW, respectively, and fully compensated losses.
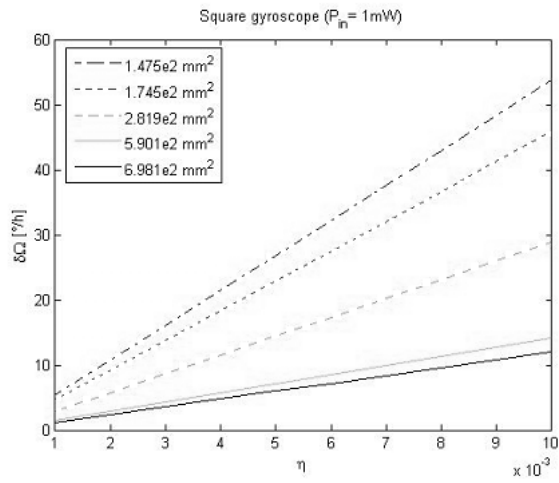
(a)

(b)

(c)

Fig. 5. Sensitivity versus coupling coefficient at λ = 1.55 μm, (a) P_{in} = 1 mW, (b) P_{in} = 10 mW and (c) P_{in} = 25 mW; full losses compensation.

From this figure we can see that the performance of the sensor is as better as the coupling coefficient is lower at a fixed value of A. We can focus on a certain value of the coupling coefficient and of the area, as an example $\eta = 0.002$ and $A = 1.475 \ 10^2$ mm^2. In this case the device sensitivity is slightly higher than $10°$/h for $P_{in} = 1$mW, becomes $4°$/h if $P_{in} = 10$ mW and further reduces to a value slightly lower than $2°$/h when $P_{in} = 25$ mW. The performance is enhanced by increasing both the input power and the resonator size and reducing the coupling efficiency.

The previous observations appear more clear if the following tables are examinated; in each table the resonant characteristics and the sensitivity are detailed for 5 different values of size and three different input powers at three different values of the coupling coefficient. L_S is the length of the straight waveguides and R_C is the curvature radius.

Square	$A = 1.475 \ 10^2$ mm^2	$A = 1.745 \ 10^2$ mm^2	$A = 2.819 \ 10^2$ mm^2	$A = 5.901 \ 10^2$ mm^2	$A = 6.981 \ 10^2$ mm^2
FWHM	$1.372 \ 10^7$	$1.267 \ 10^7$	$1.021 \ 10^7$	$7.220 \ 10^6$	$6.640 \ 10^6$
Q	$1.410 \ 10^7$	$1.527 \ 10^7$	$1.895 \ 10^7$	$2.681 \ 10^7$	$2.915 \ 10^7$
R_C, L_S	5mm, 3mm	5mm, 4mm	7mm, 4mm	10mm, 6mm	10mm, 8mm
dΩ					
$P_{in} = 1$ mW	53.77 °/h	45.84 °/h	28.93 °/h	14.14 °/h	12.00 °/h
$P_{in} = 10$ mW	17.00 °/h	14.50 °/h	9.14 °/h	4.47 °/h	3.80 °/h
$P_{in} = 25$ mW	10.75 °/h	9.17 °/h	5.79 °/h	2.83 °/h	2.40 °/h

(a)

Square	$A = 1.475 \ 10^2$ mm^2	$A = 1.745 \ 10^2$ mm^2	$A = 2.819 \ 10^2$ mm^2	$A = 5.901 \ 10^2$ mm^2	$A = 6.981 \ 10^2$ mm^2
FWHM	$6.856 \ 10^6$	$6.321 \ 10^6$	$5.094 \ 10^6$	$3.601 \ 10^6$	$3.312 \ 10^6$
Q	$2.827 \ 10^7$	$3.062 \ 10^7$	$3.799 \ 10^7$	$5.375 \ 10^7$	$5.844 \ 10^7$
R_C, L_S	5mm, 3mm	5mm, 4mm	7mm, 4mm	10mm, 6mm	10mm, 8mm
dΩ					
$P_{in} = 1$ mW	26.82 °/h	22.86 °/h	14.43 °/h	7.05 °/h	5.99 °/h
$P_{in} = 10$ mW	8.48 °/h	7.23 °/h	4.56 °/h	2.23 °/h	1.89 °/h
$P_{in} = 25$ mW	5.36 °/h	4.57 °/h	2.89 °/h	1.41 °/h	1.20 °/h

(b)

Square	$A = 1.475 \ 10^2$ mm^2	$A = 1.745 \ 10^2$ mm^2	$A = 2.819 \ 10^2$ mm^2	$A = 5.901 \ 10^2$ mm^2	$A = 6.981 \ 10^2$ mm^2
FWHM	$1.366 \ 10^6$	$1.262 \ 10^6$	$1.017 \ 10^6$	$0.719 \ 10^6$	$0.661 \ 10^6$
Q	$1.416 \ 10^8$	$1.534 \ 10^8$	$1.903 \ 10^8$	$2.693 \ 10^8$	$2.928 \ 10^8$
R_C, L_S	5mm, 3mm	5mm, 4mm	7mm, 4mm	10mm, 6mm	10mm, 8mm
dΩ					
$P_{in} = 1$ mW	5.35 °/h	4.56 °/h	2.88 °/h	1.41 °/h	1.19 °/h
$P_{in} = 10$ mW	1.69 °/h	1.44 °/h	0.91 °/h	0.44 °/h	0.38 °/h
$P_{in} = 25$ mW	1.07 °/h	0.91 °/h	0.57 °/h	0.28 °/h	0.24 °/h

(c)

Tab 1. Resonant characteristics and sensitivity at $\lambda = 1.55$ μm, (a) $\eta = 0.01$, (b) $\eta = 0.005$ and (c) $\eta = 0.001$; full losses compensation

In each table it clearly appears that the best performance can be obtained by increasing the resonator size and the input power and that performance is as better as the coupling coefficient is lower at fixed values of area and perimeter. It is also quite clear that when losses are fully compensated and the value of coupling coefficient is < 1, the resonator is characterized by a very high Q factor.

Then, the desired performance can be obtained by appropriately tailoring the coupling coefficient, the input power, and the resonator size. This trend is confirmed for all the resonator geometries. As an example, at λ = 1.55 μm, with η = 0.005, a minimum angular velocity of about 5 °/h can be theoretically achieved with an area lower than 2.9 10^2 mm^2 for all geometries and P_{in} = 10 mW. Of course, the situation is getting more and more relaxed if a sensitivity > 5 °/h is required.

READOUT TECHNIQUE

To detect the rotartion rate and the direction in which the sensor is rotating, a push-pull interference process [11] as sketched in Fig. 6a, can be used.

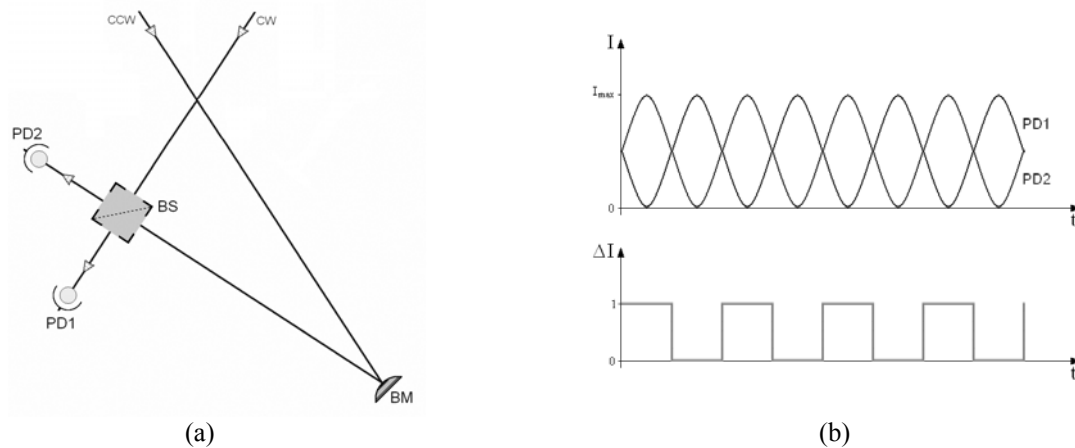(a)   (b)

Fig. 6. (a) push-pull interference scheme; (b) output signal at both the photodiodes (up) and signal at the comparator output (bottom)

The beam splitter divides the intensity of the clock-wise (CW) mode in two equal portions. The counter clock-wise (CCW) beam is deflected by a mirror and separated in two equal beams, in such a way those beams overlap with the corresponding ones of the CW beam and interferee on each photodiode. The two photodiodes are placed to give the interference pattern detected by the photodetector PD$_1$ out of phase by 180° as compared to that one at PD$_2$. In Fig. 6b the output signals at both the photodetectors, resulting from the interference, for 100% contrast case are reported. A comparator switches from 1 to 0 or from 0 to 1 when the two electrical signals have the same amplitude. When the sensors rotates in CW direction the frequency of the interference patterns will increase while when the rotation is in CCW direction the frequency decreases. In both cases the comparator output will change also in frequency; this variation will provide an evaluation of the angular velocity and of the rotation sense.

CONCLUSIONS

Currently a large use of inertial navigation systems (INS) is limited by the system stability and high cost. INS technology needs to be improved by means of high- performance sensors together with advances in terms of memory and throughput in computer technology and post-processing electronics. At the same time, high-performance space applications require reduced power, cost, size and weight.

This requirements seems to be matched by the new configuration of PRRG technology proposed. This new device has shown very promising theoretical results with an expectation of rotation rate of a few °/h.

The AVS performance has been evaluated in case of fully compensated resonator losses; the analysis has been carried out by changing the ring size, the input power and the coupling coefficient at the operating wavelength 1.55 μm.

Best obtained performance was 0.24 °/h for P_{in} = 25 mW or 0.38 °/h for P_{in} = 10 mW, respectively, at η = 0.001 while, increasing η to 0.005, the minimum detectable angular velocity of 1.20 °/h at P_{in} = 25 mW or 1.89 °/h for P_{in} = 10 mW, has been obtained.

REFERENCES

[1] European Patent EP 1219926 *"Integrated optical angular velocity sensor",* by M. N. Armenise, M. Armenise, V. M. N. Passaro, F. De Leonardis, Politecnico di Bari, filed on 28.11.2000.

[2] M. N. Armenise, V. M. N. Passaro, F. De Leonardis, M. Armenise, "Modeling and Design of a Novel Miniaturized Integrated Optical Sensor for Gyroscope Applications", *J. Lightwave Technology*, vol. 19, n. 10, pp. 1476-1494, 2001.

[3] C. Ciminelli, F. Peluso, M. N. Armenise, "Sensor Modelling", ESA IOLG Project Report, November 2004.

[4] C. Monovoukas, A.K. Swiecki, F. Maseeh, "Integrated optical gyroscopes offering low cost, small size and vibration immunity", *Intellisense Corp. Report*, 2000, http://www.intellisense.com/contentfiles/devicetechnologypapers/IntegratedOpticalGyroscopesofferinglowcostsmallsizeandvibrationimmunity.pdf

[5] C. Ford, R. Ramberg, K. Johnson, " Cavity Element for Resonant Micro Optical Gyroscope", IEEE AES Systems Magazine, pp. 33-36, December 2000.

[6] J. T. A. Carriere, J. A. Frantz, S. Honkanen, R. K. Kostuk, B. R. Youmans, E. A. J. Vikjaer, " An Integrated Optic Gyroscope Using Ion-Exchanged Waveguides", IEEE LEOS 2003, Vol. 1, pp. 99-100, October 2003.

[7] G. Li, K. A. Winick, E. A. J. Vikjaer, " Design, Fabrication and Characterization of an Integrated Optic Passive Resonator for Optical Gyroscopes", ION 60th Annual Meeting 2004, June 2004.

[8] K. Suzuki, K. Takiguchi, K. Hotate, "Monolithically Integrated Resonator Microoptic Gyro on Silica Planar Lightwave Circuit", *J. Lightwave Technology,* vol. 18, n. 1, pp. 66-72, 2000.

[9] C. Ciminelli, F. Peluso, M. N. Armenise, "A new integrated optical angular velocity sensor", SPIE Conference on "Integrated Optics: Devices, Materials, and Technologies IX", San Jose (USA), January 2005.

[10] C. Ciminelli, F. Peluso, E. Armandillo, M. N. Armenise, "Modeling of a new integrated optical angular velocity sensor", OPTRO 2005, Parigi, 9 – 12 Maggio 2005.

[11] W. Luhs, "Laser gyro experiment", January 2000, www.meos.com